NUMERICAL AND EXPERIMENTAL INVESTIGATION OF PLUMES INTERACTING WITH SATELLITE WALLS

J. Allègre[*], A. Chaix[*], I.A. Chirokov[~], N.G. Gorchakova[#], I.A. Graur[~], C. Purpura[*],
I. Gibek[+], T.G. Elizarova[~], J.-C. Lengrand[*]

Laboratoire d'Aérothermique du Centre National de la Recherche Scientifique
1C av. de la recherche scientifique, 45071 Orléans Cedex 2, France (Fax: +33 2 38 25 77 77)
AC: Tel.+33 2 38 25 77 30, chaix@cnrs-orleans.fr
JCL: Tel.+33 2 38 25 77 19, lengrand@cnrs-orleans.fr

~ Institute for Mathematical Modeling, Russian Academy of Sciences
Miusskaya sq. 4a, 125047 Moscow, Russia (Fax: +7 095 972 07 23)
IAG: +7 095 973 03 85, graur@imamod.ru
TGE: +7 095 972 11 59 telizar@yahoo.com

 # Institute of Thermophysics, Siberian Branch of Russian Academy of Sciences
1, Prosp. Acad. Lavrentyev, Novosibirsk, 630090, Russia (Fax: +7 2832 343480)
NGG: +7 3832 39 15 46 agor@bionet.nsc.ru

+ Centre National d'Etudes Spatiales
18 av. Edouard Belin, 31401 Toulouse Cedex 4, France (Fax: +33 5 61 28 29 92)
IG: +33 5 61273497 Isabelle.Gibek@cnes.fr

Abstract. Experiments have been carried out in a vacuum chamber to study twin-plumes and a single plume interacting with satellite walls. Twin-plumes were issued from two parallel conical nozzles that simulated satellite control thrusters and were operated simultaneously. Experimental investigations concerned flowfield density determination by means of electron beam surveys and wall pressure measurements. In parallel, preliminary calculations demonstrated the feasibility of numerical treatment of these configurations based on so-called quasigasdynamic equations. Both experiment and calculation indicate the absence of a recirculation zone between the nozzles.

CONTEXT OF THE STUDY

Scientific and technological space missions using micro or mini-satellites are generating growing levels of interest. Such missions complement large-scale programs and can respond more quickly to special science needs or new technologies.

CNES has been developing new platforms for micro-satellites (satellites whose total launch mass is about 120 kg) and for mini-satellites (satellites whose total launch mass is about 500 kg). The platform for mini-satellites is called PROTEUS ("Re-configurable Platform for Observation, TElecommunications and Scientific Uses").

These platforms are designed to lower costs, so that it is possible to carry out a greater number of experiments. They will be valuable tools for space experimentation and for rapid demonstrations of the feasibility of new concepts. Their in-orbit lifetime will be about three years.

Micro-satellite platform

The micro-satellite product line project started owing to a strong demand from the French science community. The platform is being designed for the broadest possible spectrum of applications, built whenever possible around standard subsystems to minimize development costs.

There will be two missions per year starting in 2002. The first selected missions are DEMETER ("Detection of Electro-Magnetic Emissions Transmitted from Earthquake Regions") in 2002 and PICARD (without hydrazine propulsion) in 2003.
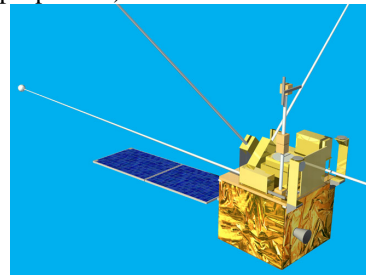
FIGURE 1. DEMETER

Mini-satellite platform

The PROTEUS platform has been developed to meet the need for a greater flexibility and lower costs. It can easily be adapted from one mission to the following one, and can be offered to the international market as a competitive product.

The first satellite, which will use this platform, is called JASON. It has been developed in co-operation between CNES and NASA, in order to replace TOPEX-POSEIDON (ocean topography). It will be launched in February 2001. PICASSO-CENA (climate study) and COROT (stellar observatory) will be launched in 2003.
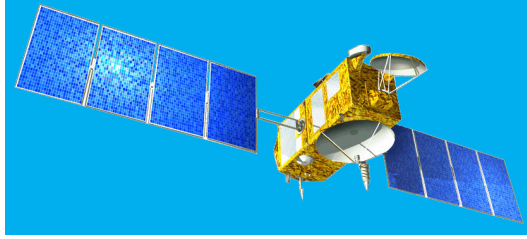
FIGURE 2. JASON

Plume effects

The propulsion subsystems of the micro-satellite platform (whenever propulsion is required) and of the mini-satellite platform are hydrazine propulsion subsystems. In particular, they are made of four thrusters (whose thrust is one Newton at the beginning of the mission). The thrusters are all located on the same side of the satellite. As the satellites are small (side of about 1mx1m for a mini-satellite, side of about 0.6mx0.6m for a micro-satellite), the thrusters are very close to one another, which is unusual. During the satellite maneuvers, they are always activated at the same time.
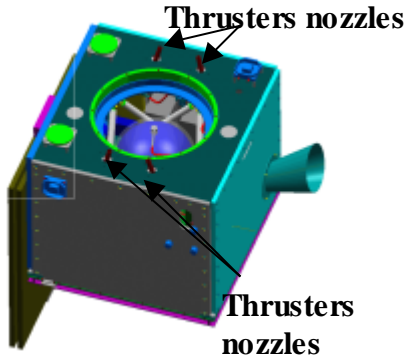
FIGURE 3. Micro-satellite hydrazine thrusters

As far as plume effects are concerned, there is not any surface in front of the thrusters plumes. But a question has been raised: is there any risk, caused by the interactions of the thrusters plumes, for the surface on which they are located? Indeed, sensitive equipment may be laid on this surface. That is why a study has been necessary. It started as an experimental work carried out in the SR3 low-density facility of the *Laboratoire d'Aérothermique du CNRS* on reduced-scale models that simulate real satellite configurations. It continues as a theoretical and numerical work to improve the prediction tools capable of treating the plume impingement problem.

EXPERIMENTAL SETUP AND CONDITIONS

Two nozzle configurations were used. The first one featured a single nozzle, and the second one consisted of twin nozzles whose axes were parallel and 50 mm apart from one another. Their main characteristics and operating parameters are given in Table 1.

The gas used for these experiments is pure nitrogen. Bird's freezing parameter characterizes the degree of non-equilibrium (or rarefaction) on the axis of a nozzle, at a given distance from the exit plane. The nozzles are made of bronze beryllium and bound up with a mechanical setup, made of stainless steel elements. This setup is mounted at the exit section of a graphite heater installed on the test chamber to heat the pressurized nitrogen flow. The heater was designed for use with only one nozzle. For the present experiments, a Y-shaped adapter allowed the simultaneous supply of two nozzles. The nozzle axis is oriented in the x-direction (Fig. 4). The origin of the x-coordinate is the nozzle(s) exit plane. The z-axis passes through the centers of the exit sections, with an origin at the center of the upper nozzle for the twin-nozzles configuration and at the nozzle center for the single nozzle configuration. The y-axis is perpendicular to both the x- and z-axes. A chromel-alumel thermocouple is mounted ahead of the convergent section of each nozzle and is connected to a digital display.

TABLE 1. Nozzle dimensions and operating parameters.

	Single nozzle	Twin nozzles
Throat radius r_c (mm)	0.2	0.2
Exit radius r_e (mm)	1.7	1.6
Half-angle of divergence	7 °	15 °
Stagnation temperature T_0 (K)	1100 ± 12	900 ± 15
Stagnation pressure p_0 (bar)	16 ± 0.04	12 ± 0.03
Molecular density n_0 (molecules.m^{-3})	1.054×10^{26}	9.657×10^{25}
Mass-flow (g.s^{-1})	0.200	2 x 0.12
Exit Mach number	5.81	5.78
Bird's parameter (at x=100 mm)	0.085	0.111

Electron beam measurements

Electron-beam diagnostics [1] have been used to determine the density field for several plume configurations. An electron beam passing through the gas excites by collisions the radiation in different spectral ranges from the X-ray region to the visible one. The intensity of this radiation is a function of the local gas density. Local measurements of radiation by the electron beam fluorescence technique (EBFT) [2] and by the X-ray e-beam method were carried out and resulted in 2-D plots of the density distribution in the jets [3]. Photographs have also been taken, by sweeping the electron beam through a given plane of the flow and collecting the resulting fluorescence. Operating conditions of the electron beam are an energy of 25 keV, a current of about 0.12 mA and a mean beam diameter of 1 mm. This diameter increases with the distance from the electron gun, as electrons collide with the molecules. The electron gun and the radiation

2

collecting systems are fixed on a solid 3-D controlled table. Table 2 summarizes the experimental configurations and the diagnostics used.
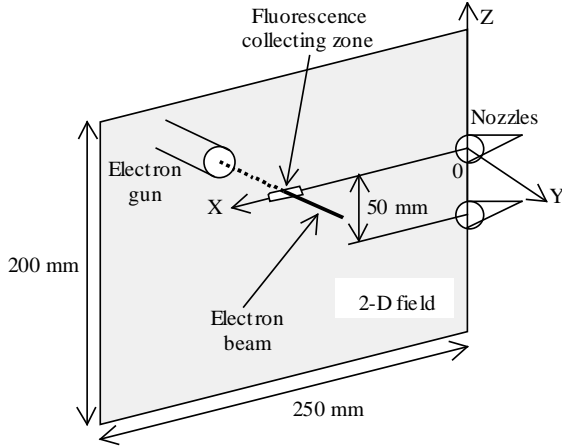
FIGURE 4. Twin nozzles and axes arrangement.

TABLE 2. Experimental work.

Experimental setup	Measurements	Diagnostics
Single nozzle	density in (x, z) plane that contains jet axis	EBFT, X-ray
Single nozzle +parallel wall (z=-17 mm)	idem	EBFT, X-ray
	wall quantities (not presented here)	• Pressure • Heat transfer rate
Twin nozzles	density in (x, z) plane that contains jet axes	EBFT, X-ray
	visualizations in planes (y, z), (x, z)	Photographs
	wall quantities	• Pressure • Heat transfer rate

The EBFT is a precise and sensitive technique at low density but a quenching effect occurs for densities higher than approximately 10^{22} molecules/m^3, resulting in a loss of sensitivity at relatively high density. Inversely, X-ray radiation is not affected by quenching, but lacks sensitivity at low density. Photographs give essentially qualitative indications on the structure of the flow [4], especially about the thickening along the x-axis of the interaction zone between the jets and about the effect of background pressure. Wall pressure and heat flux measurements give a direct indication of the flow influence on the wall.

Electron Beam Fluorescence Technique (EBFT)

Fluorescence results from the formation of N_2^{+*} excited ions by the electron beam. This non-stable state spontaneously de-excites to the fundamental state N_2^+ with the emission of a photon. The intensity of fluorescence is related to the molecular concentration in the gas. Direct excitations by primary electrons of the beam are considered. The gas is cold ($T < 1000K$) and molecules are initially in the same vibrational state $v = 0$. The spontaneous de-excitations are those which contribute to fluorescence. In the high-density regions (close to the nozzle(s)) de-excitations occur also by collision of the excited ions with N_2 molecules. The relation between fluorescence intensity and local molecular density n involves a quenching constant n_q :

$$I \propto n / \left(1 + n/n_q\right) \tag{1}$$

This constant n_q appears in the balance of the N_2^{+*} species. It depends on the collision cross-sections between N_2 and N_2^{+*}. According to different estimates [3], n_q (molecules/m^3) is in the range:

$$2.10^{-22} < n_q < 7.10^{-22} \tag{2}$$

To estimate the local molecular density n, a value of n_q has to be chosen and a reference point is needed where the intensity and the molecular density are known (subscript $_{ref}$). Then:

$$\frac{I}{I_{ref}} = \frac{n}{n_{ref}} \frac{1 + n_{ref}/n_q}{1 + n/n_q} \tag{3}$$

The local molecular density can thus be obtained as:

$$\frac{n}{n_{ref}} = \frac{\left(n_q/n_{ref}\right)\left(I/I_{ref}\right)}{1 + \left(n_q/n_{ref}\right) - \left(I/I_{ref}\right)} \tag{4}$$

To obtain the values of density and intensity at a reference point, a Pitot probe was moved along the nozzle axis ($y = 0$, $z = 0$). The local Mach number and density were obtained, based on the Rankine-Hugoniot relationships and assuming isentropic expansion from stagnation conditions to the shock wave ahead of the Pitot tube. In fact, the measured Pitot pressure is potentially affected by a lack of spatial resolution (close to the nozzle) and by an orifice effect (far from the nozzle). Therefore, two Pitot tubes with different diameters were used. The reference point was taken in a range of abscissas where both measured pressures coincide, being free of both potential errors, i.e. 40 mm $< x_{ref} < 60$ mm. The fluorescence intensity was recorded at the same locations and a value of n_q was chosen. The density profile along the nozzle axis was plotted for different choices of the reference point (from $x_{ref} = 5$ mm to $x_{ref} = 210$ mm) and different values of the quenching constant (7.10^{22} and 2.10^{22} m^{-3}). When taking $n_q = 2.10^{22}$ m^{-3}, the profiles depend strongly on the value of x_{ref}, which was considered as unrealistic. Furthermore, some values of I / I_{ref} were found larger than the maximum value $(n_q + n_{ref}) / n_{ref}$ given by Eq.3. In contrast, taking $n_q = 7.10^{22}$ m^{-3} resulted in the same density profile for any choice of x_{ref} larger than 20 mm. Therefore, the reference point was chosen at $x = 60$ mm and nq was taken equal to 7.10^{22} m^{-3}.

The exploration technique consists in displacing the whole electron gun/diagnostic apparatus along a

predefined grid. Investigating over a given plane can extend over more than one day and the electron gun has to be switched on/off, altering probably the electron beam properties. Also, a weak drift of the beam properties can occur when the electron gun runs for hours. To account for this problem, a calibration line is first recorded along the (y = cste, z = cste) line giving a $S_0(x)$ signal. Then, the exploration of the (x, z) plane is made along z-lines, at several x_i positions. The recorded signal is denoted $S_i(z)$. The displacement step is locally adapted to the expected density gradient in the x and z directions. The dark intensity S_{obc} is subtracted to each intensity measurement to obtain a value which is proportional to the fluorescence intensity. Then all z-lines are adjusted to the calibration line, according to their common point:

$$I(x_i,z) = \left(S_i(z) - S_{obs,i}\right)\frac{S_0(x) - S_{obs,0}}{S_i(z_0) - S_{obs,i}} \qquad (5)$$

Finally, the density field is obtained by applying Eq. (4).

The experimental setup for EBFT includes several lenses and a slit that collects the fluorescence emanating from a small beam element (1 mm along the beam, 3 mm across it, i.e. more than the beam diameter). Next, an interferential filter selects the fluorescence wavelength corresponding to the considered N_2^{+*} de-excitation. It is located just ahead of a photomultiplier connected to an electrometer. The measurement consists in recording a mean value of the electrometer signal during 4 seconds at each point of the exploration grid.

X-ray technique

The X-ray emission measured in the present work consists in Bremsstrahlung: a collision between an electron and a gas atom induces an X-ray photon, whose energy corresponds to the loss in energy of the electron. The process is free of quenching effects. Due to its low sensitivity, this technique was used close to the nozzle exit, where density is relatively high and quenching effect would be important in EBFT. A particular attention is necessary when measuring the signal very close to the nozzle(s): X-ray radiation coming from a solid is much larger than coming from a gas. So, if a few electrons happen to bump onto the nozzle wall, the induced radiation drowns the radiation coming from the gas. As for EBFT, the calibration of the X-ray technique was made using reference density measurements by Pitot probes. In order to obtain density values, the cosmic radiation must be accounted for:

$$I(x_i,z) = \left(S_i(z) - S_{cosm,i}\right)\frac{S_0(x) - S_{cosm,0}}{S_i(z_0) - S_{cosm,i}} \qquad (6)$$

Finally, density is obtained without quenching correction, using a reference point:

$$\frac{n(x_i,z)}{n_{ref}} = \frac{I(x_i,z)}{I_{ref}} \qquad (7)$$

The X-ray radiation detection system is essentially made of a collimator (it replaces the slit in the EBFT setup), a scintillation detector, a pre-amplifier and a recording device. The measurement technique consists in photon counting, repeated 3 or 4 times to obtain a mean value at each location. Only those photons whose energy is above a given threshold are retained.

Photographs

A series of photographs, corresponding to several (y, z) planes have been taken for twin-plumes, by sweeping the electron beam at constant speed and collecting the total radiation on a camera, the shutter staying opened. Two mirrors have been used to deflect the light and visualize planes perpendicular to the nozzle axis. The first mirror is located just under and facing the flow with an angle of 5° with respect to the vertical position. The second one just above the camera is positioned with an angle of 36° with respect to the vertical position. The focusing of the optical system was made using a target with a grid positioned successively in the visualized planes. From several grid photographs, the horizontal/vertical distortion was less than 5%.

Pressure and heat flux measurements

The aim of these measurements was to show the influence of the plume interaction on the wall between the nozzles (Fig. 5), due to a possible recirculating flow. In a first study, experiments consisted in heat flux measurements [4] between the two nozzles along the z-axis (x=0, y=0). The thin-wall technique was used. The main results will be briefly reminded. Then pressure was measured along the wall equipped with a pressure gauge. Two locations of the wall have been considered: 10 mm backward from the nozzle exit plane (position A) and flush mounted (position B). Different levels of the background pressure have been considered, most experiments being carried out for p_∞ = 1 or 2 Pa.
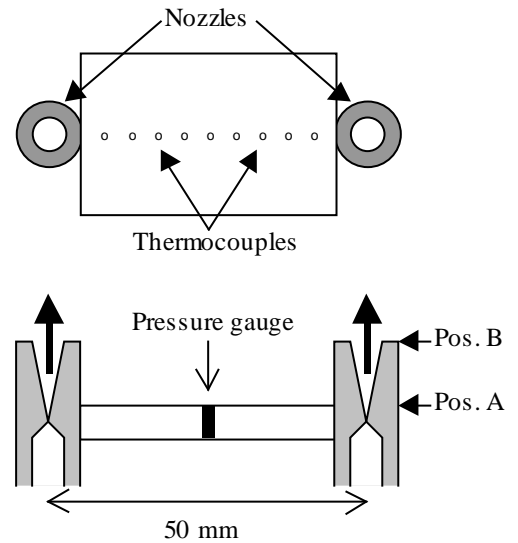
FIGURE 5. Twin-nozzle arrangement.

EXPERIMENTAL RESULTS

Electron beam measurements

The normalized density field obtained for the single nozzle is plotted in Fig.6. The range of density is very large (more than a factor of 100). In that case, it would have been very difficult to use the background gas as a reference for the EBFT measurements. Its density is low, and the intensity measurement would be strongly affected by the dark current of the photomultiplier. However, with the present calibration technique, the expected value of n_∞ / n_0 is consistent with the measured one (2.3×10^{-6}). The barrel shock due to the non-zero background pressure is clearly seen at the edge of the flow, far from the nozzle. For this nozzle configuration, 300 measurement points were necessary. The smallest z-step, close to the nozzle, was 1 mm.
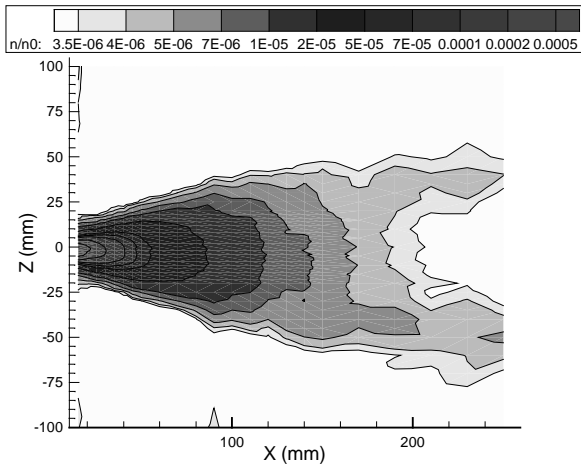
FIGURE 6. Normalized density field for the single nozzle ($p_\infty = 1$ Pa).
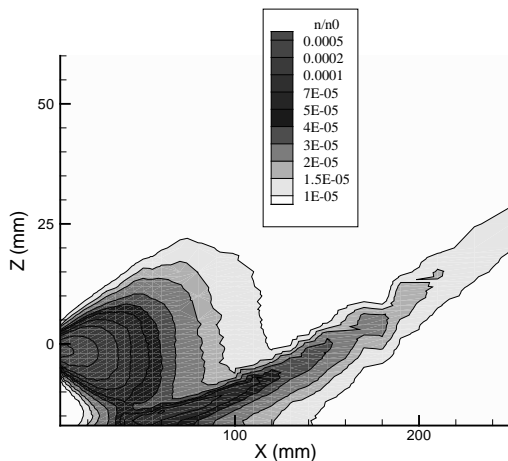
FIGURE 7. Normalized density field for the single nozzle with a parallel plate at $z = -17$ mm ($p_\infty = 1$ Pa). z-scale is larger than x-scale.

The density field for the single jet with a flat plate parallel to the nozzle axis, located at $z = -17$ mm is plotted in Fig.7. The oblique shock induced by the plate is clearly seen. Close to the nozzle exit, the density field is not modified by the wall. Close to the plate, the x-derivative of density changes sign at x ≈ 40 mm. Because the wall temperature is constant, the pressure gradient also changes sign and a flow in the negative x-direction is expected along the wall for x < 40 mm.

X-ray radiation
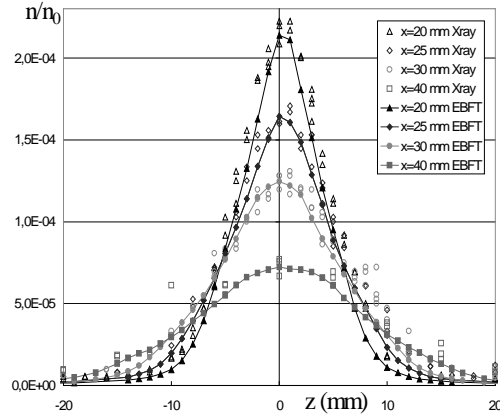
FIGURE 8. Normalized EBFT and X-ray density profiles for twin nozzles ($p_\infty = 1$ Pa).

Several profiles from both EBFT and X-ray diagnostics are plotted together in Fig.8, for twin nozzles. The good agreement between the two methods confirms that they complement each other and confirms the reproducibility of the experimental results. This good agreement makes us confident in the choice of the quenching constant.

Photographs

A series of photographs is presented in Fig. 9, corresponding to a background pressure $p_\infty = 1$ Pa. The photographs have required image processing in order to make the plume interaction more visible and to locate more precisely the external limits of the flow. The length scale of these photographs is well known, since the length of the region swept by the electron beam is 200 mm and is visible on all photographs. In contrast with photomultiplier measurements, light is not filtered. Therefore the fluorescence intensity recorded in the photograph is not related quantitatively to density, but it gives a good indication of the structure of the flow. The interaction zone enlarges when x increases. The thickness of the interaction zone is identical when estimated from the thickness of the luminous zone on a photograph or from the distance between the density peaks on a z-profile at the same x location. When the background pressure exceeds 3-4 Pa, there is no more interaction between the plumes [3]. The configuration evolves towards that of two independent plumes. This is clearly visible on visualizations in the (x, z) plane containing the jets axis. The nozzles and the interaction between the jets are clearly seen. In Fig. 10, the

background pressure was 1 Pa. This figure can be compared with the normalized density field obtained with EBFT for the twin nozzles (Fig. 11) for the same background pressure of 1 Pa. From approximately $x = 80$ mm, the density in the interaction zone is higher than on the nozzles axis.
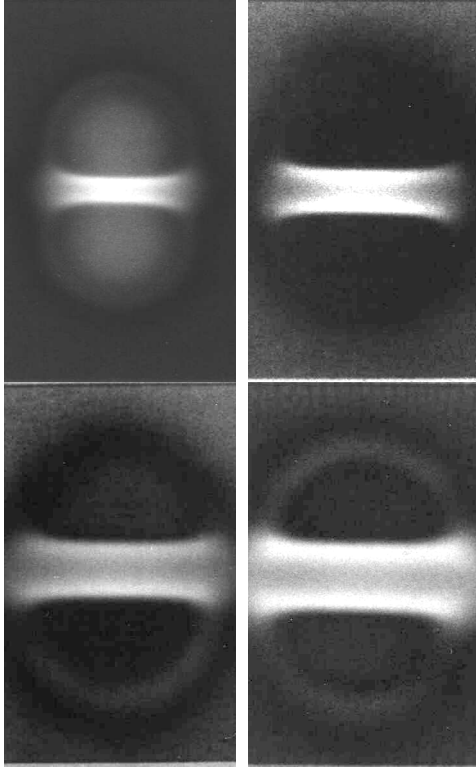
FIGURE 9. (y,z) Planes for $p_\infty = 1$ Pa at $x = 120$ mm (upper left), 180 mm (upper right), 210 mm (lower left), 240 mm (lower right).
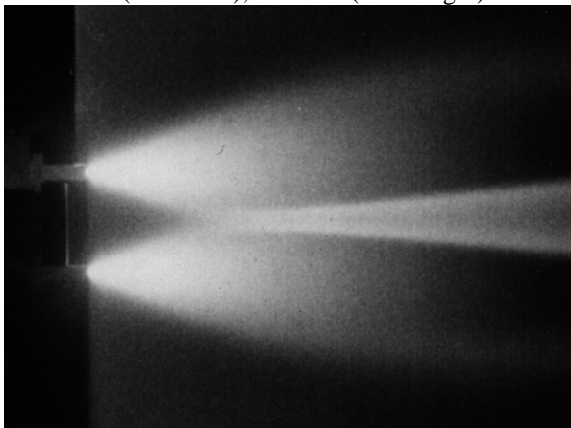
FIGURE 10. (x, z) plans for the twin nozzles configuration

Pressure and heat flux measurements

The heating rate distributions in configurations A and B are plotted in Fig.12. For a given value of p_∞, they are nearly uniform on the whole surface of the wall. Heating rates increase when pressure increases.

In a low-density gas, conduction depends on pressure, being proportional to pressure in the free

molecular limit. In the present conditions, the results suggest that the main contribution to wall heating is due to heat conduction through the gas, from the hot nozzle walls and from the hot plume interaction region. The contributions of radiation (independent of p_∞) and direct impingement of backflow (expected to increase when decreasing p_∞) seem to be negligible.
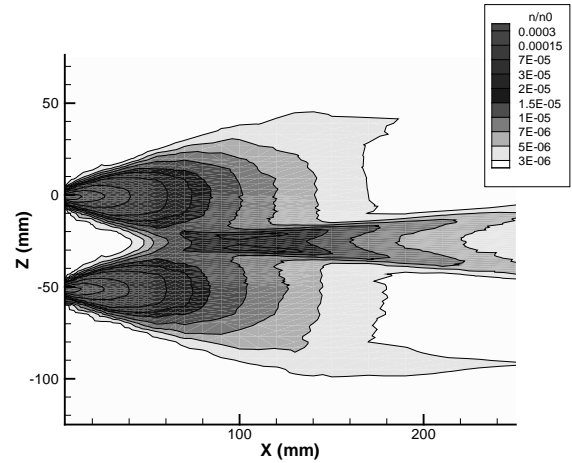
FIGURE 11. Normalized density field for the twin nozzles ($p_\infty = 1$ Pa).
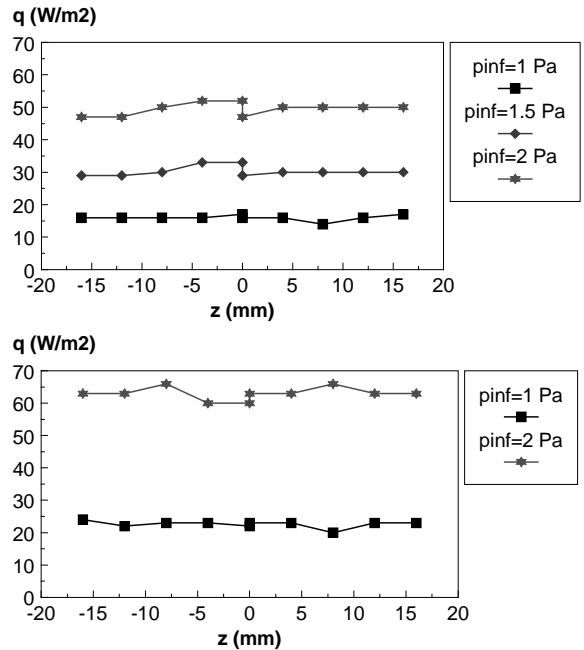
FIGURE 12. Heating rates in configurations A (top) and B (bottom) between twin-nozzles.

Wall pressure p_w was measured for two values of background pressure, 1 Pa and 2 Pa. The results obtained in the center of the wall for configurations A and B are given in Table 3.

For both positions A and B, the wall pressure is significantly lower than the background pressure, $p_w < p_\infty$. Moreover, for a same value of p_∞, p_w is even lower when the wall is located closer to the interaction zone

6

between plumes. These results attest that the wall is not submitted to a backflow effect in the conditions under investigation. Inversely, plume action induces a lowering of pressure wall with respect to the background pressure.

TABLE 3. Pressure measurements at the center of the simulated satellite wall.

	Position A		Position B	
p_∞ (Pa)	1	2	1	2
p_w (Pa)	0.42	1.09	0.32	0.77
p_w/p_∞	0.42	0.54	0.32	0.38

NUMERICAL WORK

Theoretical approach

The present work is an application of the so-called quasigasdynamic equations (QGD) which for stationary flows differ from the Navier Stokes (NS) equations by diffusive terms of order $O(Kn^2)$, where Kn is the local Knudsen number. Thus they reduce to NS equations when $Kn \rightarrow 0$. Evidence of this was given in [5] for the flow along a flat plate. Although the Direct Simulation Monte Carlo (DSMC) method is adequate to simulate non-equilibrium expansions, a continuum approach, such as solving QGD equations is of interest to compute the initial expansion close to the nozzle and provide boundary conditions to a DSMC calculation farther downstream. Also, a continuum approach is of interest to interpret experimental results obtained in ground-based facilities, where the rarefaction level is less than in real-flight conditions. In this paper, preliminary results are presented, illustrating the feasibility of QGD calculations for the problem of plume impingement.

A number of 2D and 3D problems were treated. The present paper includes only results relative to the single plume (axisymmetric) and to the twin-plume (3D) configurations, as defined above. The background pressure was taken equal to 1 Pa. The Knudsen number based on nozzle diameter and mean free path at nozzle exit is approximately equal to 4.1 x 10^{-3} for both problems.

Boundary and initial conditions

Single jet

The computational domain was a rectangle limited by the nozzle axis, the nozzle exit plane ($x = 0$), an upper limit ($r = \text{cst}$) and a downstream limit ($x = \text{cst}$).

The boundary $x = 0$ consisted of two regions:
- In the nozzle exit, boundary layer profiles of velocity and temperature were prescribed, whereas pressure was uniform. Provision was made for the divergence of the flow.
- The rest of the plane $x = 0$ was treated as an adiabatic wall.

A symmetry plane condition was imposed on the nozzle axis and so-called "soft conditions" were imposed along the upstream and downstream boundaries (*x*-derivative of velocity vector, pressure and temperature set equal to 0).

For 3D calculations (twin-plumes),

Similar boundary conditions were applied, except that the flow in the nozzle exit section was assumed parallel and uniform. Also symmetry conditions were imposed on the plane z = -25 mm, halfway between the nozzles, rather than on the nozzle axis.

For both problems, the solution was obtained by a time-convergence process, starting from a prescribed initial state.

Computational grid

Single jet

The computational domain was covered by a rectangular grid with non-uniform space steps (h^r) along the r- direction and uniform space steps (h^z) in the z-direction. In the nozzle exit section h^r is uniform and equal to $0.1r_e$. Outside the nozzle, it increases by a constant factor between adjacent cells, starting from $0.1r_e$.

For 3D calculations (twin-plumes),

The grid is rectangular with uniform space steps:
$h_x = 1.6$mm, $h_y = 0.8$ mm, $h_z = 0.8$mm.

Gas model

The calculations were carried out for Nitrogen. In QGD equations, the viscosity μ appears through a local characteristic time τ that is proportional to the mean time between collisions, and thus proportional to the local value of μ / p. In the present calculations, τ was taken constant fitted to the actual value of μ / p in the nozzle exit section.

Results

Because of the preliminary nature of the calculations, only qualitative agreement with experimental results is expected. Quantitative agreement would require more effort on grid, boundary conditions, domain size and gas modeling.

However, it can be seen in Fig.13 that the calculation reproduces the main features of the flowfield density distribution. Its upper and lower parts compare well with Figs. 11 and 6, respectively. For the twin-plume configuration, the velocity field (not plotted here) does not indicate any recirculation flow induced by the interaction region.

Wall heat transfer was not examined because the wall was supposed to be adiabatic.

The pressure distribution in the plane $x = 0$ is plotted in Fig.14 for both configurations.

For the single nozzle, the pressure decreases monotonically along the wall from the nozzle exit value to the background value.

For the twin nozzles, a low-pressure region is observed between the nozzles: wall pressure reaches values as low as $p_\infty/10$. However, on the symmetry axis ($z = -25$ mm), the pressure is close to the background

pressure p_∞. Experimentally the pressure was measured only on the axis of symmetry and was found somewhat less than p_∞. The comparison between experimental and calculated pressures should be repeated based on the definitive calculations.
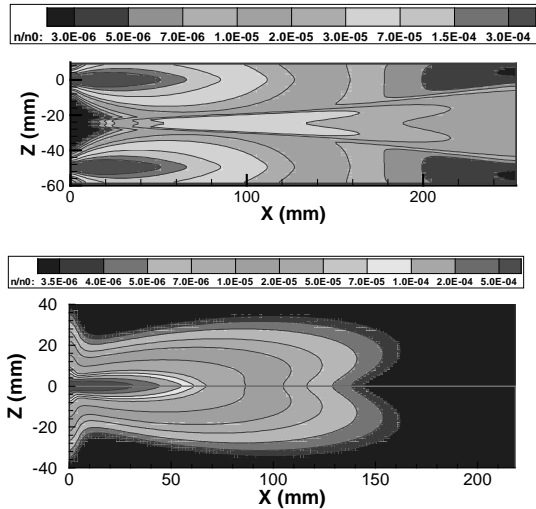
FIGURE 13. Calculated density flowfield for the twin-plumes (upper part) and single plume (lower part) at $p_\infty = 1$ Pa
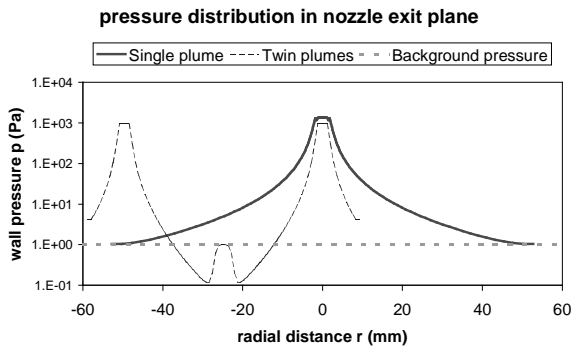
FIGURE 14. Pressure distribution in the nozzle exit plane for $p_\infty = 1$ Pa

CONCLUSION

The plumes exhausting from a thruster nozzle or from two parallel thruster nozzles have been investigated.

The distribution of density in plumes has been determined. The Electron Beam Fluorescence Technique (EBFT) has been used as the basic diagnostic technique. In the highest density regions, a quenching effect had to be taken into account to interpret the measured values of fluorescence intensity. Additional density measurements have been carried out based on X-ray emission induced by the electron beam. The measurements are free from quenching, but they are currently limited to high-density regions not too close to the nozzle. Results obtained by EBFT and X-ray technique were found consistent with one another.

Photographs have been taken in several planes perpendicular to the axis of the nozzles or containing the nozzle axes. They give rapidly a precise idea of the structure of the flow.

Pressure and heat flux measurements on the wall between twin nozzles suggest that a pumping effect generated by jets takes place instead of the expected recirculating flow with a stagnation point on the symmetry axis. Wall pressure falls below the background pressure and the heat transfer rate is constant.

Further improvement of the experiment would be a precise monitoring of the electron beam properties. In addition, replacing the classical camera by a CCD camera would make it possible to determine the density distribution in a plane by a single sweeping of the electron beam.

Preliminary numerical work based on quasigasdynamic equations has been carried out. The main features of the density flowfield have been reproduced. The calculation confirms the absence of recirculation between the twin nozzles and the presence of a low-pressure region on the wall between the nozzles.

REFERENCES

1. Allègre, J., Raffin, M., *Experimental techniques in the field of low-density aerodynamics*, AGARDograph 318(E) 1991.
2. Muntz E. P., *The electron beam fluorescence technique*, AGARDograph 132, 1968
3. Allègre, J., Chaix, A., Lengrand, J-C., *Etude expérimentale de la densité dans des jets sous-détendus*, Laboratoire d'Aérothermique du CNRS, technical note NT99-1 (1999)
4. Allègre, J., Lombardo, G., Lengrand, J-C., *Experimental study of twin-plumes interacting with a simulated satellite wall*, Proc. 3th European Symp. on Aerothermodynamics for Space Vehicles, 24th-26th Nov. 1998, ESTEC, Noordwijk, The Netherlands, ESA SP-426, Dec. 1998
5. Elizarova, T.G., Graur, I.A., Lengrand, J.C., Chpoun, A.: *Rarefied gas flow simulation based on quasigasdynamic equations*, AIAA J.,1995, 33, 12, pp. 2316-2324.